ELSEVIER

Ecological Modelling 142 (2001) 61–81

ECOLOGICAL MODELLING

www.elsevier.com/locate/ecolmodel

Comparisons of predictions of net primary production and seasonal patterns in water use derived with two forest growth models in Southwestern Oregon

N.C. Coops [a,*], R.H. Waring [b], S.R. Brown [c], S.W. Running [c]

[a] *CSIRO Forestry and Forest Products, Private Bag 10, Clayton South 3169, Melbourne, Australia*
[b] *Oregon State University, College of Forestry, Corvallis, OR 97331, USA*
[c] *University of Montana. School of Forestry, Missoula, MT 59812, USA*

Received 4 February 2000; received in revised form 1 August 2000; accepted 19 December 2000

Abstract

In this paper, we compare predictions made with two forest growth models of maximum annual net primary production and seasonal trends in the constraints imposed by different climatic variables at 18 sites in the Siskiyou Mountains of southwestern Oregon. One model, 3-PGS, is a production model driven by remote sensing data, running at monthly time steps, while the other, BIOME-BGC, is a complex eco-physiological model run at daily time steps. Both models include subroutines for predicting the interception of radiation and its dissipation as energy for evaporating water and the absorbed fraction that is photosynthetically active (400–700 nm). The models differ in a number of ways, including the estimation of canopy dynamics, calculation of respiration, use of growth modifiers and below ground mechanisms. In 3-PGS, canopy dynamics are derived from remote sensing inputs, and autotrophic respiration is assumed a constant fraction of gross photosynthesis = 0.53; in BIOME-BGC, the canopy biomass is accumulated through allocation, with respiration a function of live biomass, temperature, and nitrogen content. BIOME-BGC includes decomposition and nitrogen mineralization subroutines, while 3-PGS incorporates these processes through an index of soil fertility. Plot-based information was available at each site on species composition, site productivity, phenology, and seasonal trends in plant water relations. Long-term averages of minimum/maximum temperature and precipitation were extrapolated from local meteorological stations and converted into estimates of solar radiation, daytime vapor pressure deficits, and frequency of subfreezing temperatures for the sites, which ranged in elevation from 550 to 2135 m and had varying slopes and aspects. State-wide soil survey data were interpreted to estimate soil water holding capacity and fertility. Satellite-derived data were used to drive 3-PGS and to validate predictions of leaf area by BIOME-BCG. The two models gave similar annual estimates of total net primary production ($r^2 = 0.85$, slope = 0.64, intercept: 2.26 Mg ha^{-1} year^{-1}) but differed in their presentation of photosynthetic activity seasonally. 3-PGS has a suboptimal temperature function that provides more realistically limits on photosynthesis during the dormant season than assumed by BIOME-BGC. BIOME-BGC predicted seasonal variation in the ratio of autotrophic respiration to gross photosynthesis from 0.4 to 0.7, but over the year, the average

* Corresponding author. Fax: +61-3-95452448.
E-mail address: n.coops@ffp.csiro.au (N.C. Coops).

PII: S0304-3800(01)00279-4

was similar to that assumed by 3-PGS (0.58 ± 0.05). We discovered that Landsat imagery with 30 m spatial resolution was reasonably correlated with leaf area indices as predicted by the BIOME-BGC model, but a variation still occurred associated with small areas where outcrops of serpentine restricted canopy development.

Keywords: Climate variation; Daily and monthly models; Forest growth; Net primary productivity; Remote sensing

1. Introduction

Over the last 30 years, considerable progress has been made through the development of general models of ecosystem operation and in the way that we understand how vegetation on landscapes interact with regional and general atmospheric circulation models. Ecosystem models combine representations of plant biology, ecosystem dynamics and functions simulating, photosynthesis, stem and leaf, carbon and nutrient dynamics (Jiang et al., 1999). The models predict seasonal and interannual patterns of carbon and water vapor exchange at varying spatial and temporal resolutions and are represented by BIOMASS (McMurtrie et al., 1990), CENTURY (Parton et al., 1992), CASA (Potter et al., 1993), 3-PG (Landsberg and Waring 1997) and BIOME-BGC (Running and Hunt 1993). Where suitable micrometeorological measurements can be obtained, there is generally a good agreement between model predictions and ground observations.

There has also been a significant development in models that estimate vegetation dynamics based on remote sensing data. These models are generally used to predict existing patterns of net primary productivity (P_N) rather than predict P_N and utilize broad- and fine-scale remote sensing observations to drive the model most commonly through changing canopy function or growth. GLO-PEM, GLO-PEM 2 (Prince and Goward 1995; Goetz et al., 1999) and 3-PGS (Coops et al., 1998) are examples of this type of model. All these models share some general properties: they calculate photosynthetically active radiation intercepted by the canopy (fPAR) and estimate canopy gross photosynthesis or gross primary production (P_G), which is converted into estimates of autotrophic respiration (R_A) and P_N, and the latter partitioned to growth above- and below ground (see Table 1 for a summary of symbols and acronyms).

To apply these models, locations with homogeneous vegetation and minimal topographical variation must be delineated and site-specific meteorological data acquired. As a result of these restrictions, few ecosystem models have been tested in mountainous topography. One exception was Running (1994), who applied an ecosystem model (FOREST-BGC) to a range of sites in western Oregon where high-quality meteorological data were available along with seasonal estimates in the availability of soil water, inferred through the measurement of plant predawn water potentials (Ψ). FOREST-BGC accurately predicted seasonal variation in Ψ on drought-prone sites, given reasonable values of the total water available in the rooting zone. Similar success was

Table 1
List of acronyms and symbols used in this paper

3-PGS	Physiological principles predicting growth from satellites
α_C	Quantum canopy efficiency
θ	Mean available soil water holding capacity
ψ	Pre-dawn water potential
VPD	Vapor pressure deficit
DEM	Digital elevation model
APAR	Absorbed photosynthetically active radiation
APARu	Absorbed photosynthetically active radiation utilised
CTI	Compound topographic Index
fPAR	Fraction of photosynthetically active radiation intercepted
L	Leaf area index
NDVI	Normalized difference vegetation Index
P_A	Above ground biomass
P_B	Below ground biomass
P_G	Gross primary production
P_N	Net primary production
R_A	Autotrophic respiration

achieved with a simpler model (3-PG) developed by Landsberg and Waring (1997), which runs at monthly, rather than daily, time steps. 3-PG and a satellite-driven form of the model, 3-PGS, have been applied to forest environments in Australia and New Zealand (Landsberg and Waring, 1997; Coops 1999), South America, South Africa, UK (Waring, 2000) and North America (Landsberg et al., 2000; Coops et al., in press a).

To extend model predictions more generally into mountainous regions requires extrapolation and transformation of weather station data, and broad-scale estimates on the fertility and water holding capacity of soils. Although techniques are available to accomplish these tasks, there is rarely an opportunity to confirm how well results apply in mountainous terrain. As part of a regional study in southwestern Oregon, Coops and Waring (2000) demonstrated that 3-PGS, when initialized with satellite-derived estimates of canopy light interception (fPAR) and converted meteorological data extrapolated from weather stations, could predict the growth capacity at the same 18 sites used in this model comparison paper with an $r^2 = 0.76$ and a standard error of 0.8 $m^3\ ha^{-1}\ year^{-1}$, significant at $P < 0.01$. In addition, the process model correctly differentiated rates of soil water depletion with considerable accuracy ($r^2 = 0.78$).

Indirectly, the analysis supported the assumption that minimum/maximum temperature and precipitation data, available from many weather stations, could be successfully extrapolated across landscapes at a spatial resolution of 200 m and transformed into a complete set of climatic variables required to drive the process model: solar radiation, vapor pressure deficits, precipitation, mean and extreme temperatures. Moreover, by working with mean monthly meteorological data, averaged over 30 years, Coops and Waring (2000) demonstrated that general trends in growth and soil water depletion could be predicted across the region without requiring more detailed weather data.

With confidence in the general modeling methodology, and in our ability to extrapolate climate and soils data, we expand the approach by comparing results at the same sites with a more refined ecosystem model (BIOME-BGC) that runs at daily, rather than monthly, time steps. Satellite-derived estimates of leaf area index (L) or the fraction of light intercepted by the vegetation were acquired to initialize 3-PGS and to validate the predictions made with BIOME-BGC.

The models differ in some important ways:

1. BIOME-BGC is an eco-physiological model simulating the photosynthesis processes in plants and its response to environmental factors. It can be used as both a predictive and diagnostic tool. BIOME-BGC includes a variety of processes including new leaf growth and litterfall, snow accumulation and melting, drainage and runoff of soil water, transpiration of soil water through leaf stomata, uptake of nitrogen from the soil, decomposition of fresh plant litter and old soil organic matter, plant mortality and fire. The model employs a daily time step, allows for multiple factor interactions, and assumes that the photosynthesis process is relatively insensitive to temperatures once they rise above freezing.
2. 3-PGS is descended from the 3-PG eco-physiological model (Landsberg and Waring 1997). However, 3-PGS replies on remote sensing estimates to drive canopy dynamics and thus predicts patterns of P_N. The model employs a monthly time step and considers a single factor most limiting photosynthesis each month and the possibility that suboptimal temperatures can reduce photosynthetic capacity significantly, regardless of other factors. The importance of underlying assumptions and the advantages and disadvantages of daily versus monthly time steps are key issues in the analysis presented in this paper.

2. Methods

2.1. Study area

The Siskiyou Mountains, which extend from Southern Oregon into northwestern California, represent a steep climatic gradient with annual precipitation increasing from < 50 to 250 cm. The most widely distributed species in the region is

Table 2
Description of the 18 study plots

Stand	Elevation (m)	Slope (%)	Aspect	Parent material	Dominant vegetation
1	1490	25	W	Granite	White fir, ponderosa pine, Douglas-fir
2	1675	60	WNW	Granite	White fir, Douglas-fir
3	780	45	N	Granite	Douglas-fir, black oak, ponderosa pine
4	1920	65	SE	Ultrabasic	Jeffrey pine, incense-cedar,western white pine
5	1710	65	SE	Ultrabasic	Jeffrey pine, incense-cedar
6	2040	35	NNE	Granite	Mountain hemlock, Shasta red fir
7	1920	20	N	Granite	Shasta red fir
8	1280	40	SW	Granite	Ponderosa pine, Douglas-fir
9	1550	55	NNW	Metavolcanic	White fir, sugar pine, Shasta red fir
10	1740	55	N	Metavolcanic	Brewer spruce, Shasta red fir,mountain hemlock
11	1370	35	SW	Granite	Ponderosa pine, sugar pine, white fir,Douglas-fir
17	1830	10	E	Metavolcanic	Shasta red fir
18	2135	30	NE	Granite	Mountain hemlock
20	760	70	NNW	Mica schist	Douglas-fir, Pacific yew
21	550	75	N	Metavolcanic	Douglas-fir, black oak, Oregon white oak
22	1460	50	N	Metasedimentary	Douglas-fir, white fir
23	1400	10	N	Granite	Engelmann spruce, Douglas-fir, white fir
25	1740	5	SE	Ultrabasic	Jeffrey pine, white fir, incense-cedar,Douglas-fir

Douglas-fir (*Pseudotsuga menziesii*), but the climate is much drier than typical where the species is more dominant in the Pacific Northwest region of the United States. The geology is also more complex than elsewhere in the region with the oldest parent materials dating back to the Silurian, more than 320 million years BP. There is a full range of igneous rocks present, ranging from acidic, silica-rich granites to the most ultrabasic peridotites. In addition, the sedimentary and metamorphic rocks are widely represented. The most fertile soils are derived from graphite mica schist (Waring and Youngberg, 1972), an unusual parent material, because it contains nitrogen in its matrix (Dahlgren, 1994). The most infertile soils are derived from peridotite, and its metamorphic equivalent, serpentine.

The Siskiyou Mountains contain many endemic species, with closer ties to flora in China and the Appalachian Mountains in the eastern USA than to other areas in western North America (Whittaker, 1961). The area is particularly rich in conifers, with more than a dozen species present in some areas (Waring, 1969). Jeffrey pine, which is at its northern limits, is restricted to soils derived from peridotite and serpentine.

2.2. Plot data

Waring (1969) established an initial survey of 150 forest stands in the region and from that selected 25 stands within the eastern portion of the Siskiyou Mountains that represented the full range of vegetation, environmental, terrain and soil conditions, 18 of which were located in Oregon with the others in northwestern California. At each stand, environmental data on air and soil temperature, radiation, humidity, soil moisture, and soil fertility bioassays were acquired, but only over a few years. Tree composition and general plot descriptions are presented in Table 2. Physiological responses measured on two widely distributed conifers, Douglas-fir (*Pseudotsuga menziesii*) and Shasta red fir (*Abies magnifica* var. *shastensis*), included cell and leaf phenology, plant water potential, stomatal resistance, and foliar nutrition. Site productivity was estimated by determining maximum height of trees in mature stands and using this information to predict height and volume growth from forestry yield tables. Details of this work have been published elsewhere (Waring and Cleary, 1967; Waring, 1969; Atzet and Waring, 1970; Waring and Youngberg, 1972; Reed and Waring, 1974).

2.3. Models

2.3.1. 3-PGS

The 3-PGS (Physiological Principles Predicting Growth from Satellites) developed by Coops et al. (1998) is a simplified version of the original implementation of the 3-PG model (Landsberg and Waring 1997) and is driven primarily by vegetation light absorption, which determines the potential physiological rates. 3-PGS uses many of the principles that underlie earlier models such as FOREST-BGC (Running and Coughlan, 1988), and BIOMASS (McMurtrie et al., 1990). Like these models, 3-PGS first estimates absorbed photosynthetically active radiation (APAR). APAR is critical to 3-PGS as it provides the energy to drive the potential photosynthesis rates. APAR is computed as a product of incident PAR (photosynthetically active radiation) and the fraction of PAR absorbed by the forest canopies (*fPAR*), which is estimated from a satellite-derived index (discussed below). As APAR is a product of both PAR and *fPAR*, it will be affected by errors in either of these (Goetz et al., 1999). As a result, in order to apply the 3-PGS model, monthly estimates of *fPAR* (either from real time satellite imagery or historical records) and PAR are required. 3-PGS then calculates the utilized portion of APAR (APARu) by reducing APAR by an amount determined by the most constraining of a series of environmental modifiers that affect gas exchange through stomata: (a) high day-time atmospheric vapor pressure deficits (VPD), (b) soil water availability, and (c) the frequency of subfreezing temperatures (< -2°C). In addition, photosynthesis is further constrained by suboptimal temperatures that reduce the maximum quantum efficiency (α_c), defined by the availability of nutrients, specifically nitrogen. Gross primary production (P_G) is thus calculated at monthly time steps as the product of the amount of APARu and the 'effective' (suboptimal temperature adjusted) quantum efficiency (Landsberg and Waring, 1997).

The Penman–Monteith equation is applied to estimate transpiration from the canopy and through a water balance that considers precipitation and drainage, to estimate the change in soil water availability at monthly time steps. The model predicts outflow when soil water content exceeds the estimated storage capacity.

A major simplification in the 3-PGS is that it does not require calculation of respiration or root turnover. In 3-PGS, autotrophic respiration is assumed in temperate forests to be essentially a fixed fraction of gross photosynthesis (0.53 ± 0.04) when averaged over a month or a year (Landsberg and Waring, 1997; Waring et al., 1998). A further simplification of 3-PGS is that it partitions P_N into only two components: root and above-ground biomass. The fraction of total NPP allocated to root growth increases from 0.2 to 0.6 as the ratio APARu/APAR decreases from 1.0 to 0.2. The soil fertility index also can affect allocation if the ranking is below that of other factors for a given month.

The fraction of PAR absorbed by the forest canopies (*fPAR*) is estimated from a satellite-derived index, based on the normalised difference between reflectances measured in the near-infrared and red wavelengths, termed the normalised difference vegetation index (NDVI). This spectral vegetation index has been shown, both empirically and theoretically, to be related to the *fPAR* absorbed by vegetation canopies (Kumar and Monteith, 1982; Sellers, 1985, 1987; Goward et al., 1994).

In order to derive annual estimates of NPP, the monthly predictions of the model are simply accumulated over a 12 month period. As 3-PGS relies on continually updated estimates of PAR and *fPAR* for each month, the model does not carry the current vegetation condition forward into each new time step. The only modifier that is initialised by the previous month's condition is soil water availability, which maintains an ongoing estimate of soil moisture.

2.3.2. BIOME-BGC

The BIOME-BGC (BioGeochemical Cycles) model is a multi-biome generalization of FOREST-BGC, originally developed to simulate how a forest stand develops through a life cycle (Running and Coughlan, 1988; Running and Gower, 1991). BIOME-BGC operates at a daily time step with prescribed meteorological (maxi-

mum and minimum temperature, precipitation, humidity, and shortwave radiation) and site description information. General allometric relationships are described for seven vegetation life forms that are used to initialize plant and soil carbon and nitrogen pools. Although earlier versions of the model used satellite-derived data to estimate canopy L, the present configuration generates equilibrium estimates of L and can use satellite-derived data to confirm the validity of these estimates.

Atmospheric CO_2 is consumed during photosynthesis, which is modeled with the Farquhar photosynthesis equations (Farquhar et al., 1980). Photosynthesis is controlled by the presence or absence of a canopy, APAR, the amount and activity of leaf photosynthetic enzyme concentration, CO_2 concentration, and leaf conductance. Prescribed shortwave radiation and an exponential decay function that controls canopy light extinction determine APAR. Leaf conductance (calculated from stomatal conductance and cuticular conductance in parallel and boundary layer conductance in series) modified by a combination of environmental stresses (Jarvis and McNaughton, 1986) controls internal leaf CO_2. Maintenance respiration is subtracted from gross assimilation based on tissue N concentration and ambient temperature (Ryan, 1991). The remaining photosynthate is available for allocation to new growth to one or more of the BIOME-BGC C pools: leaf, stem, coarse root, or fine root. A fixed rate of growth respiration (30%) is assigned to each new unit of biomass produced. BIOME-BGC models production of litter and coarse-woody debris explicitly, either as litterfall and fine root turnover or through whole plant mortality.

BIOME-BGC models hydrologic processes starting with precipitation that enters the system, and estimates the amount intercepted by the canopy and litter, with the remainder stored as snowpack or infiltrating into the soil. The snowpack either melts, releasing water into the soil, or sublimates releasing vapor to the atmosphere. Water vapor leaves the system through evaporation from the soil and canopy surface or through transpiration. Water vapor fluxes, as in 3-PGS, are estimated with the Penman–Monteith equation. A one-dimensional bucket model defines the soil water holding capacity, which, when exceeded, leads to outflow. Soil water storage capacity is a function of soil type and the depth of the rooting zone. Ψ becomes increasingly more negative, and limiting, as the available water is depleted (White, 1999).

Decomposition and mineralization rates are a function of soil temperature, moisture content, and C:N ratios of litter components. Nutrient uptake is a function of pool size, mineralization rates, and transpiration. Both carbon and water cycling components of BIOME-BGC has been tested previously with success (Nemani and Running, 1989; Hunt et al., 1991; Korol et al., 1991; Pierce et al., 1993; Running, 1994; White and Running, 1994). In this paper, we use the most recently implementation of BIOME-BGC described by Thornton (1998).

2.4. Data sources for the models

2.4.1. Climate

For 3-PGS, mean monthly minimum and maximum temperature and precipitation data for the sites were derived using the PRISM (Parameter-elevation Regressions on Independent Slopes Model) software, which takes meteorological station data together with a digital elevation model (DEM) data to generate a grid of estimates of climate parameters at a resolution of 4 km^2 (Daly et al., 1994). PRISM was specifically developed to predict climate across Oregon, so the challenges of mountainous terrain played a central role in its conceptual development.

To generate mean daily observations of minimum and maximum temperature and precipitation required for BIOME-BGC, we first established relationships between quarterly seasonal PRISM estimates at each of the 18 sites with quarterly averaged long-term daily averages recorded at Ruch (Station 357391; 42°14 N, 123°02′ W, elevation 480 m), a meteorological station situated within 4 km of site No. 21. Using these scaling factors, daily changes in the patterns of precipitation and temperature were derived from the relationships shown in Fig. 1 and were the basis for extrapolation of PRISM seasonal estimates to each of the 18 sites.

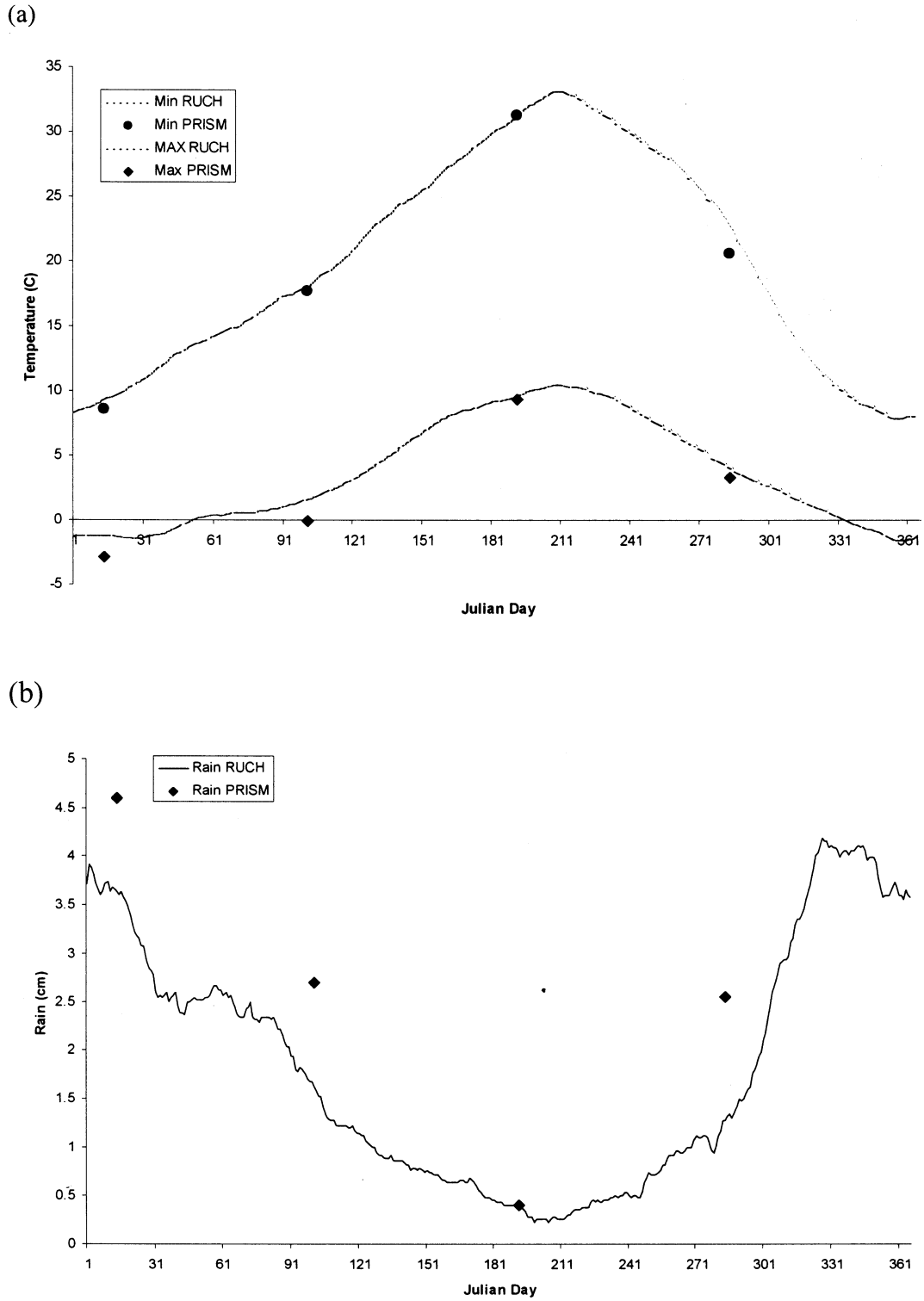

Fig. 1. (a) Mean daily observations of temperature and (b) precipitation from the Ruch station and PRISM estimates of quarterly temperatures and precipitation patterns predicted for the same location.

2.4.2. Radiation

Daily and monthly estimates of total incoming short-wave radiation were calculated using a modeling approach described by Coops et al. (in press b), which allows both diffuse and direct solar radiation to be estimated for each month based on mean daily maximum and minimum temperatures, latitude, elevation, slope, and aspect. Adjustments for differences in slope, aspect, and elevation are made by varying the fraction of diffuse and direct solar beam radiation (Goldberg et al., 1979; Bristow and Campbell, 1984; Hungerford et al., 1989). Total incoming solar radiation was modelled over the region at a 200 m spatial resolution.

2.4.3. Soil fertility and soil water holding capacity

For regional scale mapping and monitoring, the State Soil Geographic (STATSGO) database is appropriate because it has been compiled at a consistent scale for all States (United States Department of Agriculture, 1991). Soil fertility was inferred principally from the STATSGO mineralogy classes that are provided in the description of major soil types, taking into account weathering losses of minerals associated with the age of the formation. We cross-referenced fertility ranking where possible with bioassays reported by Waring and Youngberg (1972). A total of 34 mineralogy classes are reported in the STATSGO database for the USA of which 12 occur within the study area. These 12 classes were ranked from highest to lowest fertility based on expert knowledge and additional STATSGO layers including soil type and broad-scale land unit productivity. The α_c was modified as a function of soil fertility based on the work of Coops and Waring (2000) and Waring (2000). The α_c was increased linearly from 1.9 to 3.8 gC MJ^{-1} APARu (0.035–0.08 mol C mol $photon^{-1}$) over the range of fertility derived from the STATSGO dataset.

For each STATSGO soil series, the depth of each soil horizon and its mean available soil water capacity (θ) were computed and summed for the entire profile to provide an estimate of θ for each polygon. This vector coverage was then converted to raster format with a spatial resolution (size of the cell) of 250 m, approximately equivalent to a 1:250 000 scale. If an individual cell was composed of polygons representing more than one soil series, the dominant series was selected.

Zheng et al. (1996) proposed a simple model to modify θ that used the mean values of θ from the STATSGO data set, taking into account fine-scale variation on the DEM. A compound topographic index (CTI) was computed as a function of the contributing area up-slope of a central cell and the slope at that central cell on the DEM (Moore et al., 1991). Higher values of CTI tend to be found at the lower parts of watersheds and in convergent hollow areas associated with soils of low hydraulic conductivity or areas with more gentle slope than average (Beven and Wood, 1983). Soil depth and silt and clay content tend to increase from ridge tops to the valley bottoms (Singer and Munns, 1987). Soil erosion is also related to the direction of water flow, with the rates highly dependent upon the degree that soils remain saturated and the slope (Zheng et al., 1996). The model is an equation that reflects that a general positive relationship exists between CTI and θ. Zheng et al. (1996) showed that the distributions of the calculated CTI when compared to θ as obtained from STATSGO datasets were always smaller with longer tails in the high end. Thus, two scalars are needed to transform distributions of CTI into distributions of θ (Zheng et al., 1996; Coops, 2000).

2.5. Satellite data

The current AVHRR sensor on board the US National Oceanic and Atmospheric Administration's (NOAA) series of weather satellites provides data in five spectral channels from the visible, near-infrared and thermal regions of the spectrum (Kidwell, 1988). The archive accumulated from these sensors over 15 years has become a major resource in global change research following efforts by NOAA and NASA to produce a consistent processing algorithm, which has produced a carefully recalibrated and renavigated 'Pathfinder' data set (Agbu and James, 1994).

The interpretation of satellite imagery to produce vegetation attributes remains a challenging

problem with multiple factors affecting the signal recorded by the satellite sensor. Despite these difficulties, there are some clear relationships between the photosynthetic capacity of forest vegetation, regardless of species or age, and the spectral response of the vegetation in selected spectral wavelengths, in particular, the visible and near-infrared part of the spectrum. The NDVI is a commonly applied index, and, although a full explanation of the observed correlation between NDVI and canopy properties is still to be fully achieved, studies have shown that there is a linear, or near linear, relationship between *f*PAR absorbed by vegetation canopies and NDVI (Kumar and Monteith, 1982; Sellers, 1985, 1987; Goward et al., 1994). There are several limitations to such an inference, but it appears that an estimate of the amount of PAR absorbed can be estimated from NDVI and knowledge of incoming solar radiation (Prince and Goward, 1995).

Monthly, 1 km, NDVI imagery for 1995 was obtained from the Pathfinder dataset. To predict *f*PAR from NDVI, the equation developed by Goward et al. (1994) was first used over reference sites where ground-based measurements of *f*PAR were previously determined across a transect of vegetation (Runyon et al., 1994). We found it necessary to modify the slope of the relationship for 1995 AVHRR Pathfinder dataset to match the original ground-based data, and used the new equation in this study.

The new equation is:

$$\text{Fraction of PAR absorbed} = 1.67 \times \text{NDVI} - 0.08. \quad (1)$$

In applying the 3-PGS and BIOME-BGC models to pure evergreen forests in the Pacific Northwest, USA, we recognized that canopy leaf area indices and the fraction of light absorbed remain essentially stable throughout the year, at least to the extent that can be discriminated with current remote sensing technology. Because perennial vegetation tends to reach a comparable maximum value of the NDVI during mid-summer (Goward et al., 1985, 1994; Franklin et al., 1997), we calculated the maximum NDVI value from the 12 months of 1995 Pathfinder AVHRR data at each of the 18 sites and used the same maximum NDVI value for the 12 months to parameterize 3-PGS and to validate predictions of L generated by BIOME-BGC.

Table 3
BIOME-BGC input parameters[a]

Parameter	Evergreen needleleaf
Ratio of total L to one-sided L	2.4
Specific leaf area (m^2 kg C^{-1})	20.0
Aerodynamic conductance (mm s^{-1})	1.0
Maximum stomatal leaf conductance (mm s^{-1})	0.7
Water potential at stomatal closure (MPa)	−1.6
Vapor pressure deficit at stomatal closure (kPa)	2.5
Maximum photosynthetic rate (μmol m^{-2} s^{-1})	3.5
Optimum temperature (°C)	20
Leaf maintenance respiration (g kg^{-1} day^{-1})	1.2
Leaf lignin concentration (%)	27
Leaf turnover (%)	33
Maximum height (m)	30

[a] Parameters are based on total (all-sided) L.

2.6. Landsat TM satellite data

A 1995 summer Landsat Thematic Mapper scene was provided for the study region by Warren Cohen (USFS Forest Science Laboratory; Corvallis, OR). To predict *f*PAR from Landsat TM NDVI, we used the updated equation listed above and the Beer–Lambert Law inversion, assuming random foliage distribution and an extinction coefficient of 0.5, to predict L (Gower et al., 1999).

2.7. Model parameters

The initial input parameters of the two models are listed for 3-PGS and BIOME-BGC in Tables 3 and 4, respectively. To provide each of the models with an estimate of soil fertility, separate controls on soil (or leaf) nitrogen content were established. In 3-PGS, the α_c was increased linearly from 1.9 to 3.8 gC MJ^{-1} APARu over the range of fertility derived from the STATSGO

Table 4
3-PGS input parameters[a]

Parameter	Douglas fir
Boundary layer conductance (m s^{-1})	0.2
Coefficient for conductance to VPD (kPa)	−0.5
Maximum conductance stand (m s^{-1})	0.02
Extinction coefficient	0.5
Stomatal conductance coefficient (mm s^{-1})	0.005
Minimum temperature (°C)	0
Optimum temperature (°C)	20
Maximum temperature (°C)	40

[a] Parameters are based on projected surface area (0.4 of all-sided) *L*.

dataset. In BIOME-BGC, the fraction of leaf nitrogen in rubisco was used, based on the premise that the fraction of leaf nitrogen in rubisco controls potential rates of carboxylation, and is therefore the dominant control of canopy assimilation. Values for this fraction were obtained by White (1999), who undertook a sensitivity analysis on all input BIOME-BGC parameters and established mean values from the literature (see Wullschleger, 1993 for a detailed summary of possible values). These values were then also scaled over the range of fertility derived from the STATSGO dataset.

3. Results

3.1. Prediction of climate constraints on growth

Fig. 2 presents the daily and monthly climatic modifiers to growth for three contrasting sites selected from the total of 18 plots. The type dominated by Shasta red fir (*Abies magnifica* var. *shastensis*) (Site 17) is restricted to moist sites where a heavy snow pack accumulates in winter and remains until July, while the type dominated by black oak (*Quercus kelloggii*) at Site 3 occurs where water stress is sufficient to bring about early cessation of cambial activity in the summer.

Fig. 2 shows the influence of temperature, soil water availability and VPD on growth at the three sites through the year. The most important limitation to growth in the winter months is incident solar radiation, which is less than a quarter that available in mid-summer. Both models predict severe limitations on photosynthesis and growth for the oak type (site 3). BIOME-BGC predicts temperature limitations in the first three and the last two months of the year with vapor pressure deficits exerting limitations during the summer and spring months. Water stress is predicted to restrict growth with essentially no water available from days 185 to 300. The 3-PGS monthly modifiers follow similar patterns to the BIOME-BGC predictions with VPD and soil water stress restricting growth in summer. The 3-PGS temperature constraints are in evidence during the dormant season, with restrictions on photosynthesis of up 80% during the winter months, as supported by field studies where P_G was assessed through continuous monitoring of CO_2 exchange using the eddy-covariance technique (Law et al., 2000). In contrast, BIOME-BGC is far less sensitive to suboptimal temperatures, as long as they remain above freezing. An important distinction in the two models is the use of the modifiers to restrict growth at each time step. In 3-PGS, the temperature modifier affects α_c and the most restrictive modifier of soil water and VPD further limit carbon available for growth and its partitioning to above-ground production. BIOME-BGC uses all three modifiers together directly in its calculation of daily growth.

The BIOME-BGC modifiers for the site 1 with intermediate productivity show similar trends to those depicted for site 3. Soil drought, however, is less significant with water still available at the end of the summer. Site 1 has approximately similar extremes in temperature to those at Site 3. 3-PGS predicts a similar pattern of soil drought as at Site 1 with available water depleted by the end of August (confirmed by Waring and Cleary, 1967). VPD still exerts measurable constraints throughout much of the year limiting growth by 50% in the summer months.

The Shasta red fir site (Site 17) was the most productive. It experiences only minor water stress during the summer according to both BIOME-BGC and 3-PGS, as has been confirmed by measurements of predawn water potentials (Waringand Cleary, 1967). The temperature modifier, however, reduces the quantum efficiency during January by 40%, compared to 20% at the other two sites.

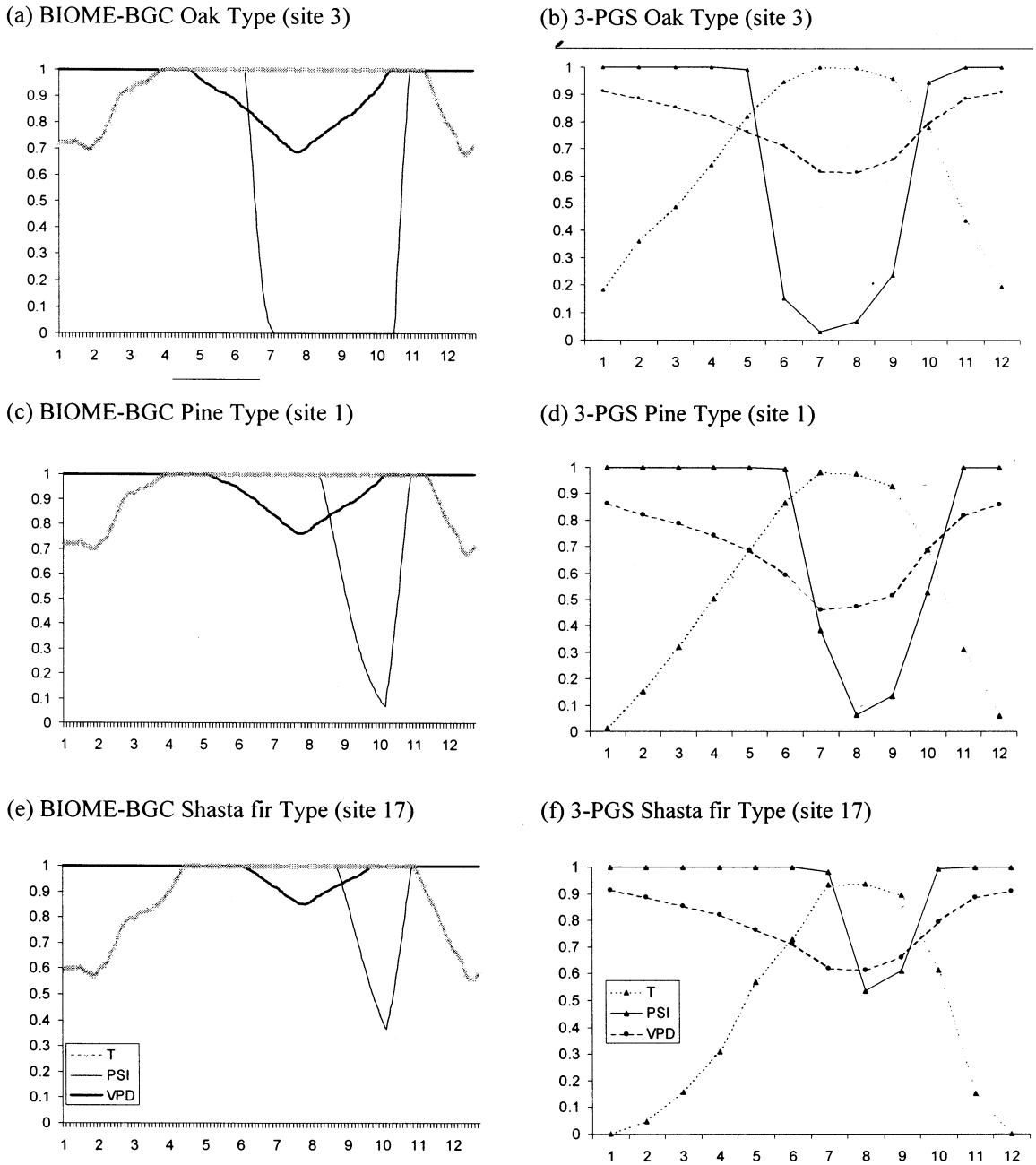

Fig. 2. Daily (BIOME_BGC) and monthly (3-PGS) climatic modifiers [temperature (T), soil water (PSI) and vapor pressure deficit (VPD)] to growth for three different forest ecosystems (Waring, 1969); (a) BIOME-BGC Oak Type (Site 3), (b) 3-PGS Oak Type, (c) BIOME-BGC Pine Type (Site 1), (d) 3-PGS Pine Type, (e) BIOME-BGC Shasta fir Type (Site 17) and (f) 3-PGS Shasta fir Type.

3.2. Modeling P_N at the three sites

Fig. 3 shows the predictions of P_N (kgC m^{-2} day^{-1}) from the 3-PGS and the BIOME-BGC models at each of the three sites. As indicated by the modifiers, site 3 is the least productive site averaging <0.004 kgC m^{-2} day^{-1} in P_N throughout the summer months with both models. Although the models predict similar patterns in P_N accumulation, 3-PGS predicts maximum growth about a month earlier than does BIOME-BGC. During the summer, BIOME-BGC predicts no P_N from day 181 to near day 300, whereas 3-PGS still indicates a modest production rate during this period.

Both models predict higher rates of production at Site 1 than at Site 3 with similar patterns through out the year. Maximum rates predicted by BIOME-BGC and 3-PGS reach 0.007 (kg C m^{-2} day^{-1}) for 3-PGS and 0.005 for BIOME-BGC. A similar decline in P_N during summer, as observed in Site 3, is predicted by BIOME-BGC. Both models predict an increase in P_N after autumn precipitation recharges the soil.

At Site 17, both models predict the highest P_N rates in summer reaching 0.008 (kgC m^{-2} day^{-1}) and 0.005 for 3-PGS and BIOME-BGC, respectively, but the patterns match less well compared to the other two sites. A more distinct seasonal peak in production is predicted with the 3-PGS model than with the BIOME-BGC. BIOME-BGC rates of growth are less constrained in winter and spring, and are slightly more restricted in summer than for 3-PGS because of greater predicted depletion of soil water and limitations imposed by high VPD. In contrast, 3-PGS predictions of P_N are much lower in the winter and spring months, but then increased and remained relatively high throughout summer and into autumn in response to differences in the rates that soil water supply is depleted. At key times throughout the year, such as around day 160 for Site 3 and day 200 at site 17, there are clear differences between the daily and monthly predictions of P_N.

3.3. Comparison of predictions of P_N at all sites

Fig. 4 compares the prediction of annual total P_N from the 3-PGS and BIOME-BGC models (in units of Mg dry mass ha^{-1} $year^{-1}$). The general correlation between the two predictions of P_N is excellent with an r^2 value of 0.85. When compared to the 1:1 line, however, there is a difference with 3-PGS estimates consistently higher than those of BIOME-BGC (Table 5). The differences are not likely to be associated with monthly vs. daily time steps. More likely, the variation in P_N rests with the differences in the estimation of *f*PAR. 3-PGS uses AVHRR-satellite-derived values to estimate *f*PAR, and these reflect all vegetation present, not just the tree component that is generated by the BIOME-BGC model. Table 5 shows the 3-PGS and BIOME-BGC predictions of P_N and L for the 18 sites.

3.4. Comparison of L predicted by 3-PGS and BIOME-BGC

Neither of the models depends on highly accurate estimates of L. In the case of 3-PGS, the key variable predicted from NDVI is *f*PAR, which increases by less than 20% once leaf area indices exceed 3.0, assuming a simple Beer Law relationship with an extinction coefficient of 0.5. BIOME-BGC requires no estimate of L; the model generates a value based on interactions with a full array of environmental factors, including atmospheric CO_2 (Thornton 1998).

Fig. 5(a) compares predictions of L estimated by conversion of *f*PAR measurements acquired with 1 km AVHRR satellite data to projected L values predicted by the BIOME-BGC. Fig. 5(b) compares predictions of L estimated by conversion of *f*PAR measurements acquired with the high spatial resolution Landsat TM imagery to those of BIOME-BGC. The close proximity of plots to one another, and the 1 km resolution of AVHRR data result in the 3-PGS predictions of L being more limited in range (2.0–4.0) than those derived from BIOME-BGC (0.2–5.0). As a contrast, Fig. 5(b) shows a greater range of LAI as predicted by the Landsat TM imagery and a slightly increased correlation coefficient value.

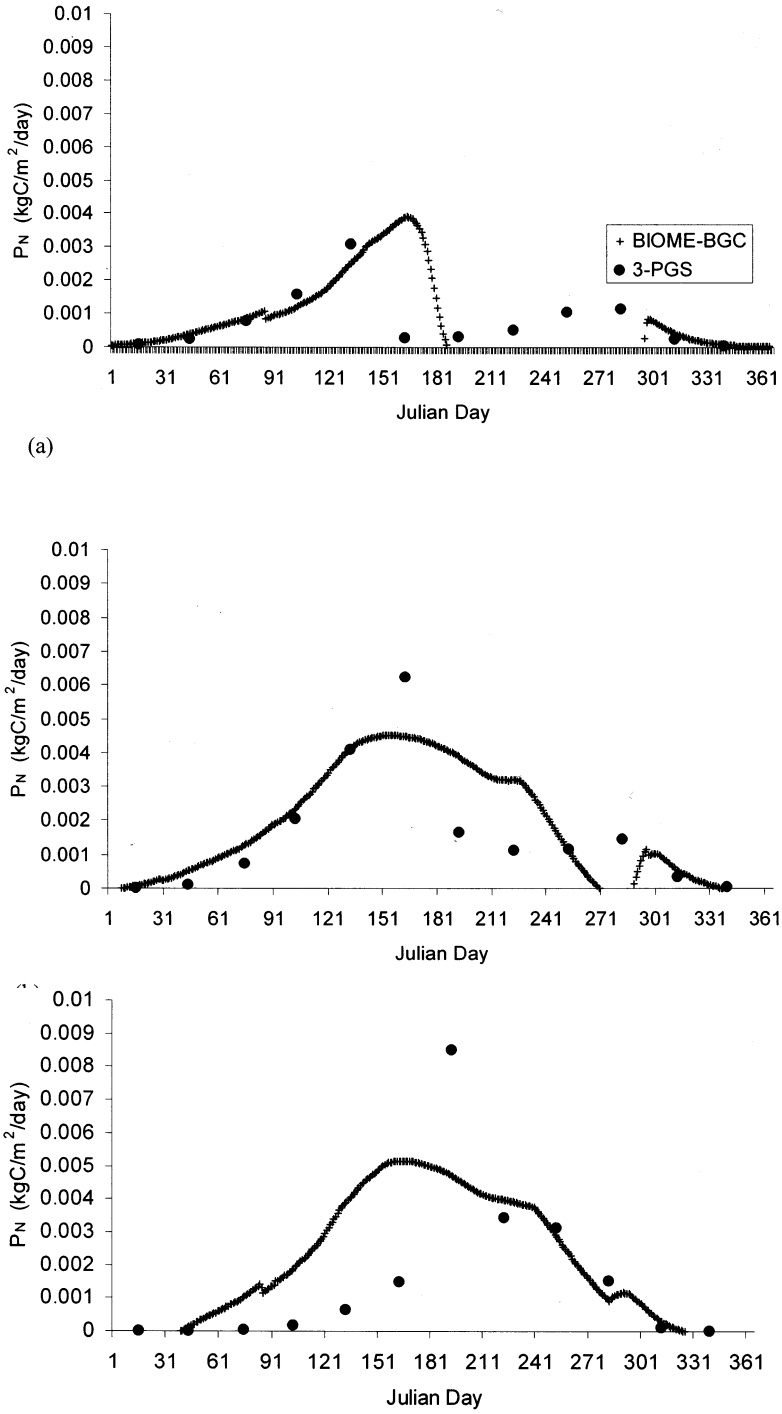

Fig. 3. Daily predictions of P_N (kgC m^{-2} day^{-1}) from BIOME-BGC (+) and 3-PGS (●) estimates, averaged for each month, for three different forest ecosystems (Waring 1969): (a) Oak Type (Site 3), (b) Pine Type (Site 1), and the (c) Shasta fir Type (Site 17).

Table 5
3-PGS and BIOME-BGC predictions of net primary production (P_N) and leaf area index (L) for the 18 sites

Dominant vegetation	Plot number	BIOME-BGC L	BIOME-BGC P_N (Mg ha^{-1} year^{-1})	3-PGS P_N (Mg ha^{-1} year^{-1})	3-PGS AVHRR L	Landsat TM L
White fir, ponderosa pine, Douglas-fir	1	3.50	6.40	6.82	3.2	2.8
White fir, Douglas-fir	2	3.00	5.46	5.84	3.3	1.8
Douglas-fir, black oak, ponderosa pine	3	1.24	2.27	3.33	2.6	2.8
Jeffrey pine, incense-cedar, Western white pine	4	0.86	1.57	3.70	2.4	1.4
Jeffrey pine, incense-cedar	5	0.58	1.00	1.68	3.0	1.7
Mountain hemlock, Shasta red fir	6	0.52	0.94	3.45	2.3	1.0
Shasta red fir	7	3.06	5.46	5.51	3.1	2.4
Ponderosa pine, Douglas-fir	8	0.85	1.59	4.50	3.0	1.5
White fir, sugar pine, Shasta red fir	9	3.40	6.08	5.98	3.5	3.3
Brewer spruce, Shasta red fir, Mountain hemlock	10	2.60	4.70	4.76	3.5	2.8
ponderosa pine, sugar pine, white fir, Douglas-fir	11	4.70	8.30	8.62	5.0	5.0
Shasta red fir	17	4.04	7.20	6.85	4.1	2.8
Mountain hemlock	18	0.90	1.75	3.70	2.3	1.4
Douglas-fir, Pacific yew	20	2.60	4.60	5.26	3.7	2.8
Douglas-fir, black oak, Oregon white oak	21	1.80	3.20	3.64	2.7	1.7
Douglas-fir, white fir	22	2.90	5.20	5.47	3.9	3.0
Engelmann spruce, Douglas-fir, white fir	23	3.30	5.95	5.71	3.5	3.3
Jeffrey pine, white fir, incense-cedar, Douglas-fir	25	4.10	7.30	6.17	3.4	3.8

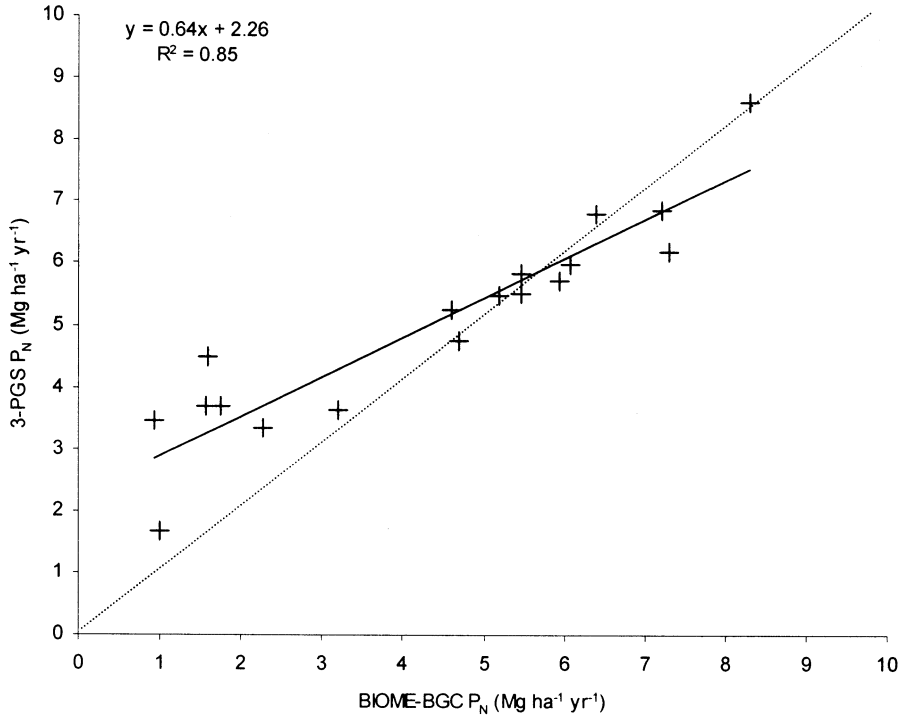

Fig. 4. Comparison of the prediction of total P_N (Mg ha^{-1} year^{-1}) from the 3-PGS and BIOME-BGC model with data points and solid line representing the regression equation. The dotted line represents a 1:1 relationship.

The difference between the two predictions arises from the ability to discern greater spatial variation in *f*PAR, and the subsequent inversion to *L*, with 30 m resolution Landsat Thematic Mapper imagery than with 1 km resolution of AVHRR data. In addition, however, an exact correspondence between the BIOME-BGC predicted potential *L* of the site (based on long-term climate averages) and the estimates of actual *L* from either 1995 AVHRR or Landsat TM imagery may not be expected. If any of the sites have been subject to short-term disturbance factors such as local drought, fire or harvesting, then a direct match between the predicted potential and the actual *L* will not exist due to reduced canopy cover below that typical for the site. Analysis of the 1995 meteorological station data indicates that 1995 rainfall was similar to the average rainfall conditions of the region (Coops and Waring, 2000), but other disturbance factors may influence this relationship. The strength of the correlations in Fig. 5(a) and (b), however, indicate that, whilst there is some variation between predicted and observed, there is generally a good correspondence with the BIOME-BGC predictions and *L* estimates from remote-sensing techniques.

3.5. P_N/P_G ratio

One of the major simplifications in the 3-PGS model that causes some concern among physiologists is the assumption of a constant R_A/P_G (or P_N/P_G) ratio (see Waring et al., 1998). The relative stability of these ratios is supported by empirical data (Waring et al., 1998; Malhi et al., 1999; Law et al., 2000) but may vary in different biomes (Ryan et al., 1997) and justifies further research.

As BIOME-BGC predicts autotrophic respiration, we compared the R_A/P_G ratio for all 18 sites. Fig. 6 shows that the monthly variation for 9 months encompassing the most active period for the 18 sites ranged from 0.4 to 0.7, with an overall

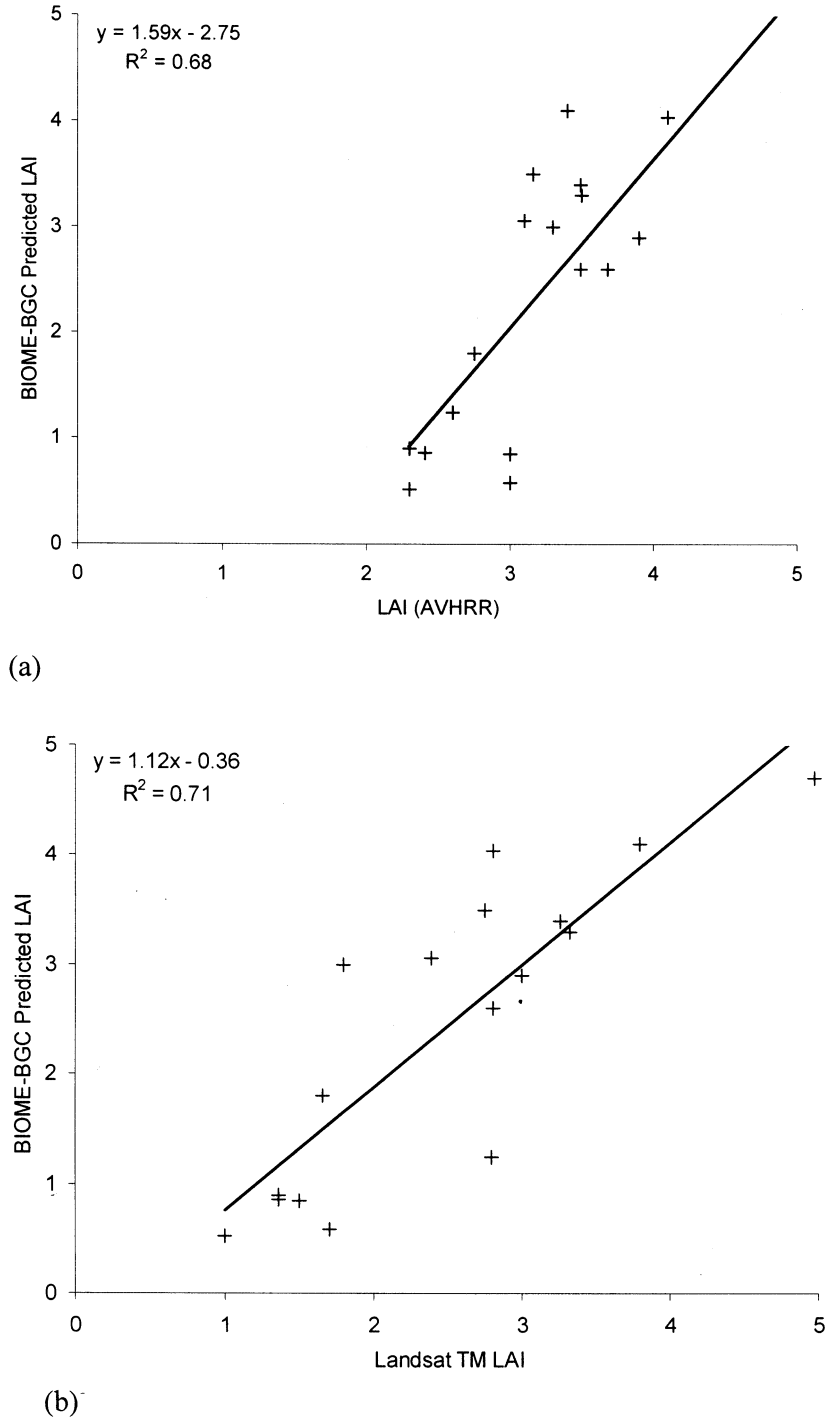

Fig. 5. Comparison of predicted projected leaf area index (L) from the BIOME-BGC against LAI as derived from (a) AVHRR and (b) Landsat TM imagery.

average of 0.58 ± 0.05, in general agreement with the value 0.53 assumed in 3-PGS.

4. Discussion

Plummer (2000) provides an overview of the incorporation of remote sensing data into ecological process models such as 3-PGS and BIOME-BGC. Plummer (2000) draws distinctions in the way remote-sensing data are utilised in these types of models providing four alternative strategies: to estimate input variables, to test and validate predictions, to update or adjust ecological models, and to apply ecological models to understand remote sensing responses.

The use of remote sensing in 3-PGS and BIOME-BGC, as discussed in this paper, demonstrates two of these four strategies. The use of AVHRR imagery in 3-PGS is a critical input data source for driving the model with the input NDVI corresponding to forcing functions or state variables in an ecological modelling context (Jørgensen, 1994). The use of remote sensing data, in this context, is perhaps the most common way to link data with ecological models (Plummer, 2000). Initially, in the development of FOREST-BGC (Running and Coughlan, 1988; Running and Gower, 1991), remote-sensing data were used in a similar fashion, but in BIOME-BGC, remote-sensing data are no longer required as an input; rather, they are used to test and validate predictions such as comparing predictions of L with the temporal and spatial variation of NDVI (Running and Nemani, 1988).

These differences in the use of remote-sensing data with the two models clearly affect their predictions, as shown in these results. 3-PGS drives its canopy dynamics from monthly (or maximum) NDVI values and thus reflects the actual seasonal variations in *fPAR* of the vegetation. BIOME-BGC, in contrast, generates daily canopy dynamics based on local climate and soil conditions. This difference is obvious (as shown in Fig. 5) with 3-PGS providing average monthly predictions, whilst BIOME-BGC provides continual daily predictions.

The debate surrounding the most appropriate time step at which to model plant growth is important (Chen et al., 1999). A primary disadvantage of longer time step is the inability to model stream flow accurately or to distinguish snow from rain when temperatures oscillate around freezing. The intensity of storms, and estimates of canopy interception, however, can be statistically incorporated into monthly time step

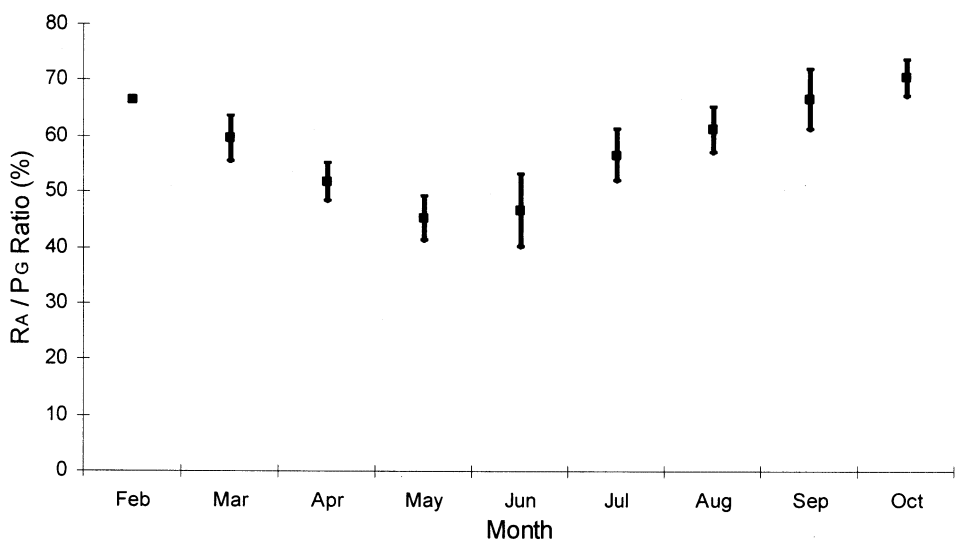

Fig. 6. Mean monthly variation (± 1 standard deviation) of the R_A/P_G ratio averaged for the 18 sites as predicted by BIOME-BGC.

models. Moreover, suboptimal temperature and lower solar radiation in the winter reduce errors in the estimation of P_G at these and higher latitudes.

A distinct advantage of models with monthly time steps is that (a) monthly weather records are more generally available and can be transformed more accurately into derived estimates of other meteorological variables at monthly time steps than daily ones; (b) monthly mean climate can also be interpolated to daily values using stochastic weather generators; (c) globally, daily climate data are extremely limited, and data accuracy can be questionable. Coops et al. (submitted for publication) evaluated the accuracy with which daily and mean monthly values of APAR, VPD, and the number of frost days in a month can be predicted using only daily and mean monthly temperature extremes, knowledge of the global location, and general equations available from the literature. They found that APAR, VPD, and the number of frost days per month predicted at monthly time steps with the same input variables gave r^2 values >0.9 and average standard errors of 0.72 MJ m^{-2} day^{-1} for APAR, 0.13 kPa for VPD, and 1.6 days per month for frequency of frost days. At daily time steps, the same equations the agreement between predicted and measured APAR and VPD were lower, with r^2s of 0.62 and 0.79, respectively.

In drought-prone areas, such as the Siskiyou Mountains, it becomes important to obtain a good estimate of rooting depth, which varies considerably with topography, soil development and parent material. We found it necessary also to make some adjustments for slope position. Where springs bring water close to the surface, even on shallow soils, the opportunity of using finer spatial resolution in satellite detection would seem feasible, but our experience suggests that adjusting survey plots to equivalent slopes, aspects, and elevations via DEMs may be more appropriate. This involves using automated search procedures that shift the initial location of each plot within specified bounds to give a closer agreement with field estimates of aspect, slope, and soil water holding capacity. This process overcomes many problems associated with correctly registering the precise location of field plots upon digitized topographic and soil maps and allows representative environmental regimes to be extrapolated across landscapes (Coops, 2000).

As soil water becomes less limiting, fertility becomes more important in restricting growth. Even with more detailed soil surveys, we might find it difficult to assess the availability of nutrients to trees. In fact, in many cases, where atmospheric deposit or intensive plantation management is practised, as in parts of the United Kingdom, it is more rewarding to obtain good climatic data and assess through modeling the potential maximum theoretical yields, compared to those measured (Waring, 2000).

Alternatively, some measure of total canopy nitrogen content would be valuable and can be obtained, at least for closed canopy forests, with fine-spatial resolution optical sensors (Matson et al., 1994). It may be possible to obtain remotely sensed estimates of canopy quantum efficiency from satellite sensors through a correlation with chlorophyll concentrations or total nitrogen content. To date, however, only aircraft have carried a fine-resolution spectrometer capable of resolving biochemical constituents of foliage from space (Matson et al., 1994; Smith and Curran, 1995; Martin and Aber, 1996).

There is little doubt that, in the future, it will be possible to obtain improved estimates of *f*PAR and other canopy properties, perhaps even measures of changes in canopy height and total above-ground biomass using LIDAR, but to estimate net carbon exchange, net accumulation in vegetation and soils, along with hydrologic properties, we will continue to be dependent on improved and widely tested models at a variety of time steps. Toward this end, it would be desirable to establish additional well-instrumented sites across broadly different landscapes and investigate how well various models generate reliable climatic data and predict measured seasonal variation in important ecosystem processes.

Acknowledgements

We thank Dr. Joe Landsberg for advice in the use of 3-PGS. Dr. Peter Thornton and Dr. Mike White (University of Montana) were extremely helpful in providing insights into the operation and parameterization BIOME-BGC. We are also grateful to Dr. John Aber and Dr. Ray Hunt for constructive criticism on early drafts of this paper and the two anonymous reviewers whose comments improved the manuscript. Part of this research was undertaken by Dr. Coops while he was on leave from CSIRO Forestry and Forest Products, Australia at the Department of Forest Science, Oregon State University. The research reported in this article was supported by funds from the National Aeronautics and Space Administration (NASA) Grant Number NAG5-7506. Additional information on this research and the 3-PGS model is available at http://www.fsl.orst.edu/bevr/ and mirrored at http://www.ffp.csiro.au/.

References

Agbu, P.A., James, M.E., 1994. The NOAA/NASA Pathfinder AVHRR Land Data set Users Manual. Goddard Distributed Active Archive Center. NASA Goddard Space Flight Center, Greenbelt.

Atzet, T., Waring, R.H., 1970. Selective filtering of light by coniferous forests and minimum light energy requirements for regeneration. Can. J. Bot. 48, 2163–2167.

Beven, K.J., Wood, E.F., 1983. Catchment geormorphology and the dynamics of runoff contributing areas. J. Hydrol. 65, 139–158.

Bristow, K.L., Campbell, G.S., 1984. On the relationship between incoming solar radiation and daily maximum and minimum temperature. Agric. Forest Meteorol. 31, 159–166.

Chen, J.M., Liu, J., Cihlar, J., Goulden, M.L., 1999. Daily canopy photosynthesis model through temporal and spatial scaling for remote sensing applications. Ecol. Modell. 124, 99–119.

Comins, H.N., McMurtrie, R.E., 1993. Long-term response of nutrient-limited forests to CO_2 enrichment; equilibrium behaviour of plant–soil models. Ecol. Appl. 3, 666–681.

Coops, N.C., 1999. Linking multi-resolution satellite-derived estimates of canopy photosynthetic capacity and meteorological data to assess forest productivity in a *Pinus radiata* (D. Don) stand. Photogramm. Eng. Remote Sens. 65, 1149–1156.

Coops, N.C., 2000. Comparison of topographic and physiographic properties measured on the ground with those derived from digital elevation models. Northwest Sci. 74, 116–130.

Coops, N.C., Waring, R.H., Landsberg, J.J., 1998. Assessing forest productivity in Australia and New Zealand using a physiologically-based model driven with averaged monthly weather data and satellite derived estimates of canopy photosynthetic capacity. Forest Ecol. Manage. 104, 113–127.

Coops, N.C., Waring, R.H. Estimating maximum potential site productivity and site water stress of the Eastern Siskiyous using 3-PGS. Can. J. Forest Res, 31, 143–154.

Coops, N.C., Waring, R.H., Landsberg, J.J., in press a. Estimation of potential forest productivity across the Oregon transect using satellite data and monthly weather records. Int. J. Remote Sens.

Coops, N.C., Waring, R.H., Moncrieff, J. Estimating mean monthly incident solar radiation on horizontal and inclined slopes from mean monthly temperatures extremes. J. Biometeorol, 44 (4), 204–211.

Coops, N.C., Phillips, N., Waring, R.H., Landsberg, J.J., submitted for publication. Prediction of solar radiation, vapor pressure deficit, and occurrence of frost from mean daily temperature extremes. Agric. Forest Meteorol.

Dahlgren, R.A., 1994. Soil acidification and nitrogen saturation from weathering of ammonium-bearing rock. Nature 368, 838–841.

Daly, C., Neilson, R.P., Phillips, D.L.., 1994. A statistical-topographic model for mapping climatological precipitation over mountainous terrain. J. Appl. Meteorol. 33, 140–158.

Farquhar, G.D., von Caenimerer, S., Berry, J.A., 1980. A biochemical model of photosynthetic CO_2 assimilation in leaves of C_3 plants. Planta 149, 78–90.

Franklin, S.E., Lavigne, M.B., Deuling, M.J., Wulder, M.A., Hunt, R.E. Jr., 1997. Estimation of forest Leaf Area Index using remote sensing and GIS data for modeling net primary production. Int. J. Remote Sens. 18, 3459–3471.

Goetz, S.J., Prince, S.D., Goward, S.N., Thawley, M.M., Small, J., 1999. Satellite remote sensing of primary production: an improved production efficiency modeling approach. Ecol. Modell. 122, 239–255.

Goldberg, B., Klein, W.H., McCartney, R.D., 1979. A comparison of some simple models used to predict solar irradiance on a horizontal surface. Solar Energy 23, 81–83.

Goward, S.N., Tucker, C.J., Dye, D.G., 1985. North American vegetation patterns observed with the NOAA-7 advanced very high resolution radiometer. Vegetatio 64, 3–14.

Goward, S.N., Waring, R.H., Dye, D.G., Yang, J., 1994. Ecological remote sensing at OTTER: Satellite macroscale observations. Ecol. Appl. 4, 322–343.

Gower, S.T., Kucharik, C.J., Norman, J., 1999. Direct and indirect estimation of leaf area index, fAPAR and net primary production of terrestrial ecosystems. Remote Sens. Environ. 70, 29–51.

Hungerford, R.D., Nemani, R.R., Running, S.W., Coughlan, J.C., 1989. MTCLIM: A Mountain Microclimate Simulation Model. Paper INT0414. United States Department of Agriculture Research, Ogden, UT 52 pp.

Hunt, E.R. Jr., Martin, F.E., Running, S.W., 1991. Simulating the effects of climatic variation on stem carbon accumulation of a ponderosa pine stand: comparison with annual growth increment data. Tree Physiol. 9, 161–171.

Jarvis, P.J., McNaughton, K.G., 1986. Stomatal control of transpiration: scaling up from leaf to region. Adv. Ecol. Res. 15, 1–49.

Jiang, H., Apps, M.J., Zhang, Y., Peng, C., Woodard, P.M., 1999. Modelling the spatial pattern of net primary productivity in Chinese forest. Ecol. Modell. 122, 275–288.

Jørgensen, S.E., 1994. Fundamentals of Ecological Modelling. Elsevier, Amsterdam.

Kidwell, K.B., 1988. NOAA Polar Orbiter Data TIROS-N, NOAA-6, NOAA-7, NOAA-8, NOAA-9, NOAA-10, NOAA-11 User's Guide. National Oceanic and Atmospheric Administration.

Korol, R.L., Running, S.W., Milner, K.S., Hunt, E.R. Jr., 1991. Testing a mechanistic carbon balance model against observed tree growth. Can. J. Forest Res. 21, 1098–1105.

Kumar, M., Monteith, J.L., 1982. Remote sensing of plant growth. In: Smith, H. (Ed.), In Plants and the Daylight Spectrum. Academic Press, London, pp. 133–144.

Landsberg, J.J., 1986. Physiological Ecology of Forest Production. Academic Press, Sydney 198 pp.

Landsberg, J.J., Gower, S.T., 1997. Applications of Physiological Ecology to Forest Management. Academic Press, San Diego, CA 354 pp.

Landsberg, J.J., Waring, R.H., 1997. A generalized model of forest productivity using simplified concepts of radiation-use efficiency, carbon balance, and partitioning. Forest Ecol. Manage. 95, 209–228.

Landsberg, J.J., Johnsen, K.H., Albaugh, T.J., Allen, H.L. McKeand, S.E., in press. Applying 3-PG, a simple process-based model designed to produce practical results, to data from loblolly pine experiments. Forest Sci.

Law, B.E., Waring, R.H., Anthoni, P.M., Aber, J.B., 2000. Measurements of gross and net ecosystem productivity and water vapor exchange of a *Pinus ponderosa* ecosystem, and an evaluation of two generalized models. Global Change Biol. 6, 155–168.

McMurtrie, R.E, Rook, D.A., Kelliher, F.M., 1990. Modeling the yield of *Pinus radiata* on a site limited by water and nitrogen. Forest Ecol. Manage. 30, 381–413.

Malhi, Y., Baldocchi, D.D., Jarvis, P.G., 1999. The carbon balance of tropical, temperate and boreal forests. Plant Cell Environ. 22, 715–740.

Martin, M.E., Aber, J.D., 1996. Estimating forest canopy characteristics as inputs for models of forest carbon exchange by high spectral resolution remote sensing. In: Gholz, H.L., Nakane, K., Shimoda, H. (Eds.), The Use of Remote Sensing in the Modeling of Forest Productivity. Kluwer Academic, Dordrecht, pp. 61–72.

Matson, P., Johnson, L., Billow, C., Miller, J., Pu, R., 1994. Seasonal patterns and remote spectral estimation of canopy chemistry across the Oregon transect. Ecol. Appl. 4, 280–298.

Moore, I.D., Grayson, R.B., Ladson, A.R., 1991. Digital terrain modeling — a review of hydrological, geomorphological and biological applications. Hydrol. Process. 5, 3–30.

Nemani, R.R., Running, S.W., 1989. Testing a theoretical climate–soil–leaf area hydrologic equilibrium of forests using satellite data and ecosystem simulation. Agric. Forest Meteorol. 44, 245–260.

Parton, W.J., McKeown, R., Kirchner, V., Ojima, D.S., 1992. CENTURY User's Manual. Natural Resource Ecology Laboratory, Colorado State University, Ft. Collins, CO 289 pp.

Pierce, L.L., Walker, J., Dowling, T., McVicar, T.R., Hatton, T.J., Running, S.W., Coughlan, J.C., 1993. Ecohydrological changes in the Murray–Darling basin, III, A simulation of regional hydrological changes. J. Appl. Ecol. 30, 283–294.

Plummer, S.E., 2000. Perspectives on combining ecological process models and remotely sensed data. Ecol. Modell. 129, 169–186.

Potter, C.S., Randerson, J.T., Field, C.B., Matson, P.A., Vitousek, P.M., Mooney, H.A., Klooster, S.A., 1993. Terrestrial ecosystem production: a process model based on global satellite and surface data. Global Biogeochem. Cycles 7, 811–841.

Prince, S.D., Goward, S.M., 1995. Global primary production: a remote sensing approach. J. Biogeogr. 22, 815–835.

Reed, K.L., Waring, R.H., 1974. Coupling of environment to plant response: A simulation model of transpiration. Ecology 55, 62–72.

Running, S.W., 1994. Testing FOREST-BGC ecosystem process simulations across a climatic gradient in Oregon. Ecol. Appl. 4, 238–247.

Running, S.W., Coughlan, J.C., 1988. A general model of forest ecosystem processes for regional applications. I. Hydrologic balance, canopy gas exchange and primary production processes. Ecol. Modell. 42, 125–154.

Running, S.W., Nemani, R., 1988. Relating seasonal patterns of AVHRR vegetation index to simulated photosynthesis and transpiration of forests in different climates. Remote Sens. Environ. 24, 347–367.

Running, S.W., Gower, S.T., 1991. FOREST-BGC, a general model of forest ecosystem processes for regional applications. II Dynamic carbon allocation and nitrogen budgets. Tree Physiol. 9, 147–160.

Running, S.W., Hunt, E.R. Jr., 1993. Generalization of a forest ecosystem process model for other biomes. BIOME-BGC and an application for global scale models. In: Ehleringer, J.R., Field, C. (Eds.), Scaling Physiological Processes: Leaf to Globe. Academic Press, San Diego, CA, pp. 141–158.

Runyon, J., Waring, R.H., Goward, S.N., Welles, J.M., 1994. Environmental limits on net primary production and light-use efficiency across the Oregon transect. Ecol. Appl. 4, 226–237.

Ryan, M.G., 1991. Effects of climate change on plant respiration. Ecol. Appl. 1, 157–167.

Ryan, M.G., Lavigne, M.B., Gower, S.T., 1997. Annual carbon cost of autotrophic respiration in boreal forest ecosystems in relation to species and climate. J. Geophys. Rev. 102 (D24), 28871–28883.

Sellers, P.J., 1985. Canopy reflectance, photosynthesis and transpiration. Int. J. Remote Sens. 68, 1335–1372.

Sellers, P.J., 1987. Canopy reflectance, photosynthesis, and transpiration 2. The role of biophysics in the linearity of their interdependence. Remote Sens. Environ. 21, 143–183.

Singer, M.J., Munns, D.N., 1987. Soils: An Introduction. Macmillan, New York, pp. 336–337.

Smith, G.M., Curran, P.J., 1995. The estimation of foliar biochemical content of a slash pine canopy from AVIRIS imagery. Can. J. Remote Sens. 21, 234–244.

Thornton, P.E., 1998. Description of a numerical simulation model for predicting the dynamics of energy, water, carbon, and nitrogen in a terrestrial ecosystem. Ph.D. Dissertation, University of Montana, Missoula, MT.

United States Department of Agriculture, 1991. State Soil Geographic Data Base (STATSGO). Soil Conservation Service, Miscellaneous Publication No. 1492. Washington, DC.

Waring, R.H., Cleary, B.D., 1967. Plant moisture stress: evaluation by pressure bomb. Science 155, 1248–1254.

Waring, R.H., 1969. Forest plants of the eastern Siskiyous: their environmental and vegetational distribution. Northwest Sci. 43, 1–17.

Waring, R.H., Youngberg, C.T., 1972. Evaluating forest sites for potential growth response of trees to fertilizer. Northwest Sci. 46, 67–75.

Waring, R.H., Landsberg, J.J., Williams, M., 1998. Net primary production of forests: a constant fraction of gross primary production? Tree Physiol. 18, 129–134.

Waring, R.H., 2000. A process model analysis of environmental limitations on the growth of Sitka spruce plantations in Great Britain. Forestry 75, 65–79.

White, J.D., Running, S.W., 1994. Testing scale dependent assumptions in regional ecosystem simulations. J. Veg. Sci. 5, 687–702.

White, M.A., 1999. Monitoring and modeling growing season dynamics. Ph.D. dissertation, University of Montana, Missoula, MT.

Whittaker, R.H., 1961. Vegetation history of the Pacific Coast States and the 'central' significance of the Klamath region. Madrono 16, 5–23.

Wullschleger, S.D., 1993. Biochemical limitations to carbon assimilation in C3 plants — a retrospective analysis of the A/Ci curves from 109 species. J. Exp. Biol. 44, 907–920.

Zheng, D., Hunt, E.R., Running, S.W., 1996. Comparison of available soil water capacity estimated from topography and soil series information. Landscape Ecol. 11, 3–14.